VISUALIZATION AND ANALYSIS OF FULL-WAVEFORM AIRBORNE LASER SCANNER DATA

Å. Persson *, U. Söderman, J. Töpel, S. Ahlberg

Department of Laser Systems, Swedish Defence Research Agency, P.O. Box 1165, SE-58111 Linköping, Sweden - (asa.persson, ulf.soderman, johanna.topel, simon.ahlberg)@foi.se

Commission III, WG III/3

KEY WORDS Airborne laser scanning, LIDAR, laser data processing, waveform digitization, waveform analysis, point extraction

ABSTRACT:

Recent development of airborne laser scanner systems allows for digitization and recording of the full-waveform, i.e. the received signal of the reflected laser pulse. In this paper, some visualizations and analysis of waveform data are presented. The purpose is to study how waveform data can be used to extract additional information. As a first step, 3D point data are extracted and parameterized. The approach for extracting 3D point data is based on unsupervised learning where a mixture of Gaussian distributions are fitted to the waveforms to detect the peaks using the EM algorithm. The performance of this approach is compared to the real-time processing echo extraction by the system. The number of points extracted per waveform is studied and examples will illustrate where additional points have been extracted.

1. INTRODUCTION

Airborne laser scanning (ALS) is a well established technique for acquiring detailed 3D data of the natural environment. Today, most ALS systems produce data in terms of 3D point clouds. The 3D coordinates of the positions where the laser pulses are reflected in the environment are determined using laser range measurements (the time-of-flight) and the position and orientation of the platform. The position and orientation data are obtained from differential GPS and INS (Inertial Navigation System) subsystems. Most systems have the ability to detect and record multiple returns from a single laser pulse, usually first and last return. Multiple returns typically occur at building edges and in vegetation, e.g. one part of the laser beam may be reflected from the top of the tree and some part within the tree and/or the ground surface.

A new feature in the next generation commercial systems is the possibility for digitization and recording of the full-waveform, i.e. the received signal of the reflected laser pulse. Already in the 80th and 90th, some systems having this capability were developed. In 1981, the development of the FLASH/HawkEye laser bathymetry system started at the Swedish Defence Research Agency (Steinvall et al., 1981), and in 1994, the HawkEye system was made operational by SAAB (Steinvall et al., 1994). Another system, used for vegetation mapping (Blair et al., 1999), is the SLICER system which was built by NASA. Work on waveform analysis has been performed using data from these systems (Hofton et al., 2000; Tulldahl et al., 2000).

Three commercial topographic mapping systems which allow for full-waveform digitization have recently emerged on the market: the TopEye Mark II system (www.topeye.com), the LiteMapper 5600 build around the Riegl LMS-Q560 (www.riegl.co.at), and the Optech Inc ALTM 3100 system (www.optech.on.ca). These new systems open up new possibilities for data analysis. Now, the end user can elaborate on and test various pulse detection methods. Previously, pulse detection has been proprietary of the ALS manufacturer and not available for manipulation by the end user.

The waveform data opens up possibilities for extracting additional and more detailed information from the data in an off-line processing step. The data provides the possibility for a more detailed description of the structure of objects and more accurate range measurements. For example, low vegetation may be separated from ground and canopy height measurements may be improved (Hug et al., 2004). Also, the waveform data allows for extracting multiple return data.

In this paper, waveform data from the TopEye Mark II system is studied. One approach for visualizing waveform data is presented together with a number of illustrating examples. Also, analysis of waveform data is performed. The aim is to extract additional information associated with the reflections caused by objects in the laser pulse travelling path. For example, additional 3D points are extracted and their spatial distribution is studied. In this paper, an approach based on unsupervised learning is presented where a mixture of Gaussian distributions are fitted to the waveforms to detect and parameterize the peaks. This approach uses the Expectation Maximation (EM) algorithm (Dempster et al., 1977). Many different optimization techniques exist. In (Hofton et al., 2000), a similar algorithm is presented which decomposes waveform data into a sum of Gaussian components. The fitting of the Gaussian components are based on a nonlinear least-squares method (LSM).

Four small test areas with different type of vegetation were selected for illustrating the results. The performance of this approach to extract additional 3D points is compared to the

---

* Corresponding author.

airborne laser scanner system's real-time processing for point extraction. The number of points extracted per waveform is shown and examples will illustrate where additional points have been extracted.

2. LIDAR DATA

The data acquisition was performed during the fall 2004 using the new TopEye ALS system. The data set covers the Remningstorp forest estate in the south of Sweden and contains both point and waveform data. The data was collected using the first version of the new TopEye Mark II system. This system operates at a wavelength of 1064 nm and the pulse rate is 50 kHz. The scanner system uses a rotating mirror producing an elliptical scan pattern on ground, a.k.a. Palmer scan (Wehr, A. and Lohr, U. 1999). The scanner rotation speed was 35 revolutions per second. The flight altitude was about 200 m, the pulse length 5 ns and the beam divergence 1 mrad. The point density in the surveyed area was about 25 points/m^2. The system produced up to two returns per laser pulse, first and last return.

The waveform data was recorded from the time of the last return and 127 samples earlier, using 8 bits per sample. The waveform digitization frequency was 1 GHz resulting in a distance between the samples of 0.15 m. The X, Y, and Z - coordinate of the first value in the waveform as well as its direction vector were provided (Figure 1).
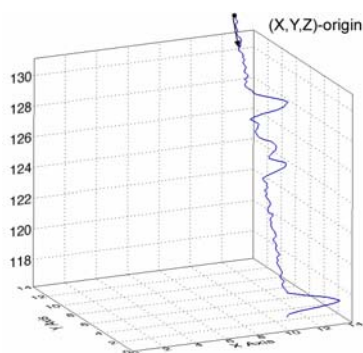

Figure 1. The waveform data was recorded in the mode 'last echo and earlier'. Each waveform contains 128 samples which correspond to about 19.2 meters. The first coordinate of the waveform (X,Y,Z-origin) and its direction vector were provided.

The system uses two separate receiver channels with different amplification to obtain a large dynamic range. In this first version of the system, the recordings were from every second channel independently of which waveform that was actually used to detect the laser return. Thus, some waveforms (around 35 %) contained only noise and were removed when analysing the data. This recording scheme from every second channel will be changed in future versions of the system and a new version is already announced during preparation of this paper.

3. VISUALIZATION

To facilitate interpretation and to enhance understanding of waveform data, 3D visualization was used. The waveform samples were inserted in a 3D volume consisting of small 3D cells referred to as voxels (volume elements, compare with pixels = picture elements in the 2D case). The voxel size

(length, width, height) was set to 0.15 m. For each sample, the voxel containing its 3D coordinate was located and the amplitude of the sample was assigned to the voxel. If more than one sample was associated with the same voxel, the sample with the highest amplitude value was selected.

Four small areas (15m x 15m) were selected for visualizing and analysing the waveform data. The areas consisted of (1) pine trees, (2) spruce trees, (3) deciduous trees, and (4) a road surrounded by grass and some trees. In Figure 2, the waveform data for the areas are visualized. Note that the vegetation gives rise to many vertical distributed returns compared to the open area with the road.
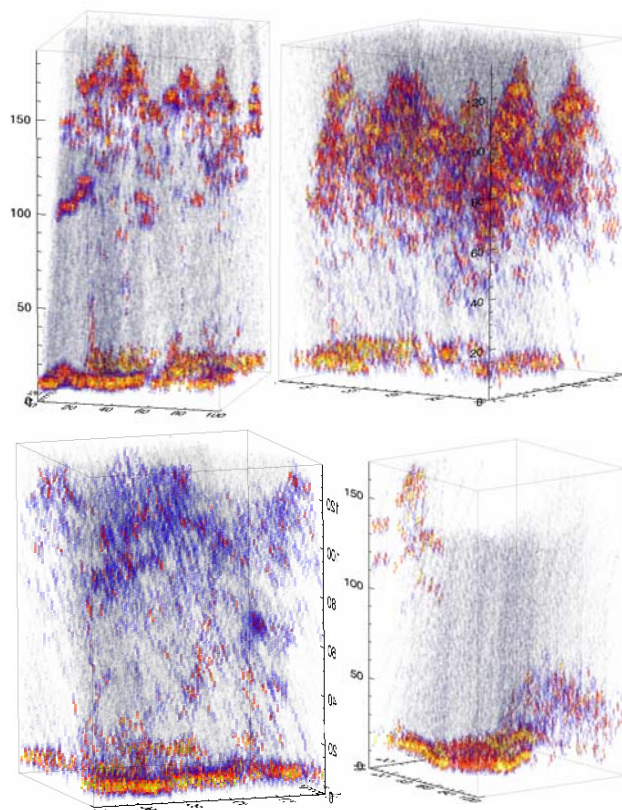

Figure 2. Volumes with waveform data. Area 1 (top left), area 2 (top right), area 3 (lower left), area 4 (lower right). The transparency is linear such that low values are more transparent. Voxel size: 0.15x0.15x0.15m^3.

4. ANALYSIS

4.1 Method

As a first step to extract additional information from the waveform data, such as 3D points, the peaks in the waveforms were detected and parameterized. To detect the peaks, Gaussian distribution functions were fitted to the waveforms. The waveform was modelled as a sum of Gaussian distributions

$$\hat{y} = f(x) = \sum_{j=1}^{k} p_j \times f_j(x) \quad (1)$$

where $f_j(x) \sim N(\mu_j, \sigma_j^2)$

and p_j is the relative weight of the component distribution $f_j(x)$.

To determine the number of components that best described the data is part of the unsupervised learning problem. For each waveform, a range of components were fitted, k_{min} to k_{max}. The minimum number of components that were fitted was one and the maximum nine. For each component, j, the mean (μ_j), the standard deviation (σ_j), and relative weight (p_j) were estimated using the EM algorithm (Oliver et al., 1996). Then, a criterion was used to compare the models. The k-value that minimized the criterion was chosen.

4.2 EM algorithm

The maximum likelihood estimates for p_j, μ_j and σ_j were calculated by iterating through the following equations

$$Q_{ij} = \frac{p_j f_j(i)}{\sum_{j=1}^{k} p_j f_j(i)} \quad (2)$$

$$p_j = \frac{\sum_{i=1}^{S} N_i Q_{ij}}{\sum_{i=1}^{S} N_i} \quad (4)$$

$$\mu_j = \frac{\sum_{i=1}^{S} N_i Q_{ij} i}{p_j \sum_{i=1}^{S} N_i} \quad (5)$$

$$\sigma_j = \sqrt{\frac{\sum_{i=1}^{S} N_i Q_{ij} (i - \mu_j)^2}{p_j \sum_{i=1}^{S} N_i}} \quad (6)$$

where $Q_{ij} =$ the probability that sample i belongs to component j
$N_i =$ the intensity for sample i
$S =$ the number of samples in the waveform

4.2.1 Pre-processing. Before applying the EM algorithm to the waveforms, the noise was first removed by calculating a threshold for each waveform. The threshold was based on calculating the standard deviation of the noise, σ_{noise} (equation 7). The σ_{noise} was calculated by computing the median absolute deviation (*MAD*) (www.vostat.org/help/median_mad_and_ quantile.html) of the waveform. The *MAD* is a measure of the dispersion of a distribution about the median. The *MAD* is multiplied by a factor of 1.4826 to achieve consistency with the standard deviation for asymptotically normal distributions.

$$\sigma_{noise} = 1.4826 \cdot median(| waveform - m |) \quad (7)$$

$$m = median(waveform)$$

The median, m, was subtracted from the waveform and the result was divided by a multiple of the noise deviation, σ_{noise}. Then, all samples of the waveform below the multiple of σ_{noise} were set to zero in the original waveform. Samples just below the threshold, on each side of a peak(s), were added to the waveform as long as the amplitude value was lower than its neighbouring samples. Figure 3 shows an example of a waveform where the noise has been removed (dashed line).

Start values. To generate good estimates of μ_j, σ_j, p_j, the initial values are important. The start values for μ_j were chosen by using local maxima in a slightly smoothed version of the waveform. The first initial value was placed at the position of the local maxima belonging to the part of the waveform with the widest return (greatest number of consecutive nonzero samples). This process was repeated for the remaining components. If more components were used than there were peaks in the waveform, the process started over again but this time with a shift of two samples from the local maxima. The start values for σ_j were set to two and p_j were set so all components started out with an equal weight. In Figure 3, the start values when five components will be estimated are shown.
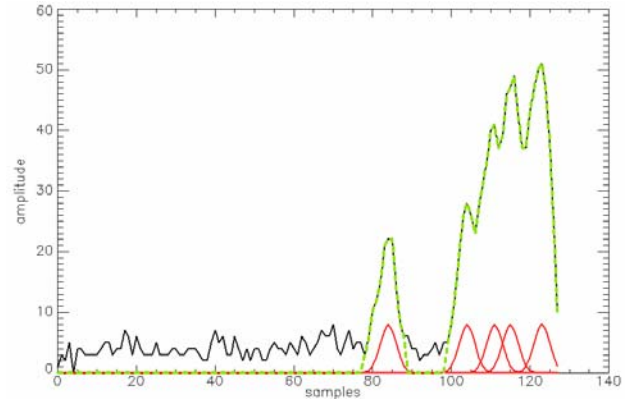

Figure 3. Waveform data (black solid) and pre-processed waveform (gray dashed). The gray solid lines show the start values when five components will be estimated.

4.3 Estimating the number of components

Several different criteria can be used to estimate the number of components, $k_{min} \leq k \leq k_{max}$, that best describes the data (Oliver et al., 1996). In this approach, the Akaike's Information Criterion (*AIC*) (Gustafsson, 2000) was used

$$\hat{k} = \arg\min_k \log(V_S(k)) + \frac{2k}{S} \quad (8)$$

$$V_S(k) = \frac{1}{S} \sum_{i=1}^{S} (y_i - \hat{y}_i)^2$$

where y is the waveform and $\hat{y}$ is the sum of the Gaussian distributions. The k-value yielding the minimum value of the criterion was used. The denominator in the loss term, the last term in equation 8, was set to five in this case. Further work will be to also test other criteria.

Restrictions were set to the range of k-values that were estimated. The minimum number of components (k_{min}) that were estimated was set to the number of local maxima found. The maximum number of components (k_{max}) that were estimated for a waveform depended on the distance between the components. When too many components were estimated, the components ended up close together. The minimum distance between two components was set to 5.33 samples (0.80 m). When the distance between two components was smaller than 5.33 samples, the estimation stopped and no more components were estimated. In Figure 4, the estimated components are shown for the waveform in Figure 3. The amplitude of the components is normalized by the area of the waveform.
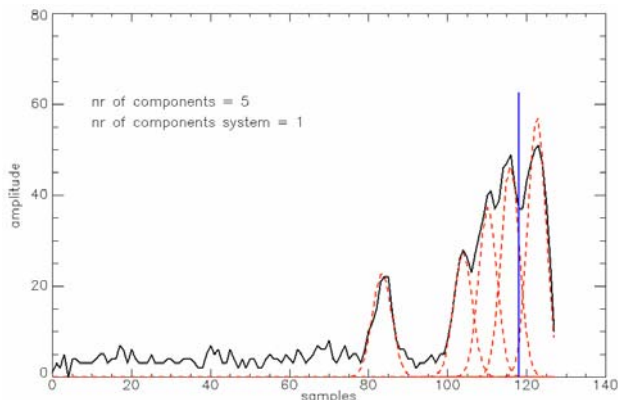
Figure 4. Waveform data (solid) and five estimated components (gray dashed), μ_1=83.65, μ_2=103.89, μ_3=110.02, μ_4=115.99, μ_5=122.60. The vertical line symbolizes the position of the point extracted by the system.

4.4 Extraction of 3D points

The estimated models can be used more or less directly to extract information from the waveforms, such as extraction of point data. One point was associated with each component distribution. In an initial attempt, the points were defined as follows: μ_j was used as the position of the point, $2*\sigma_j$ was used as the width of the point, and the amplitude of the waveform (y) at the mean value ($y(\mu_j)$) was used as the intensity of the point. Note that these points also contain information about the width of the waveform peak that gives rise to the point.

The number of points extracted using the waveforms was compared to the points extracted by the system (the method used for pulse detection by the system is not known). Only those points derived by the system corresponding to recorded waveforms containing real data (i.e. not only noise) were used in the comparison. Each extracted point was also linked to the closest point extracted by the system. By studying non-linked points, information of where additional points have been extracted was provided.

5. RESULTS AND DISCUSSION

The point data set from the TopEye system consisted of first and last return. The waveform data gave the possibility to extract more than two returns per laser pulse. In Table 1, the extracted number of points per waveform is summarized for the three forest areas (1-3).

A total of 4127, 4997 and 5007 points were extracted for area 1-3 which were 18%, 30% and 57% more respectively than the points delivered by the system. In Figure 5, the number of points extracted per waveform (*) is compared to points extracted by the system (◊) from the corresponding waveforms for the three areas.
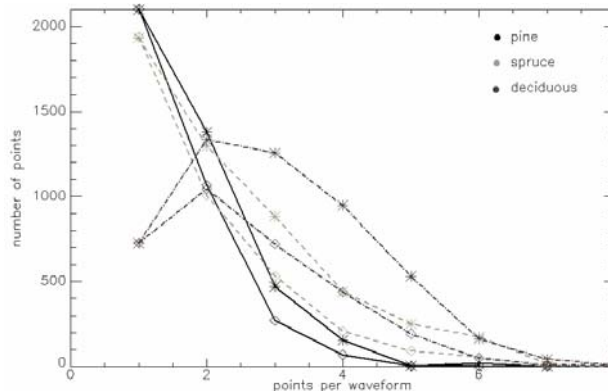

Figure 5. Extracted points by system (◊) and from waveform data (*). Pine (black solid), spruce (light gray dashed), deciduous (gray dash-dotted).

Figure 6 shows point clouds for the three forest areas. The first column shows the points extracted by the system, the middle column shows the points extracted from the waveforms and the third column shows the additional points extracted from the waveforms.
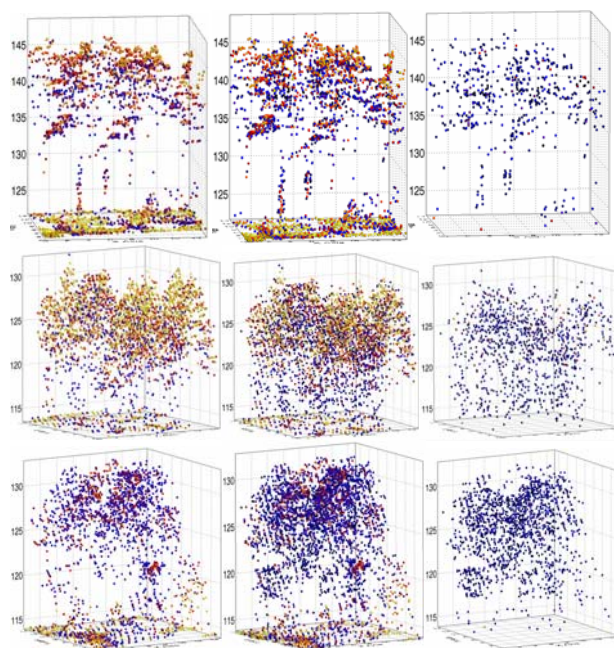

Figure 6. Point clouds for area 1-3, (15m x 15m). Pine trees (top row), spruce trees (middle row) and deciduous trees (bottom row). Extracted points by system (left column), from waveform data (middle column), and additional points extracted from waveform data (right column). The color indicates the intensity of the point.

Note that the majority of the additional points were obtained from reflections in the tree crowns or in the understory. This

Area	Pine		Spruce		Deciduous	
Points extracted per waveform	Nr of waveforms	Nr of points	Nr of waveforms	Nr of points	Nr of waveforms	Nr of points
0 (noise)	1601 (35%)		1242 (29%)		1556 (42%)	
1	2099 (70%)	2099	1933 (63%)	1933	726 (33%)	726
2	689 (23%)	1378	648 (21%)	1296	667 (30%)	1334
3	157 (5%)	471	294 (10%)	882	419 (19%)	1257
4	39 (1%)	156	110 (4%)	440	237 (11%)	948
5	1 (0.03%)	5	50 (2%)	250	106 (5%)	530
6	3 (0.1%)	18	29 (0.9%)	174	27 (1%)	162
7	0	0	2 (0.07%)	14	6 (0.3%)	42
8	0	0	1 (0.03%)	8	1 (0.05%)	8
9	0	0	0	0	0	0
	2988 waveforms	4127 points (18 %)	3067 waveforms	4997 points (30 %)	2189 waveforms	5007 points (57 %)

Table 1. Number of extracted points from waveform data.

conforms to what could be expected, that vegetation give rise to many vertical distributed returns but open areas only one distinct return.

Up to eight points were extracted from a waveform. This can lead to a better description of the vertical structure of vegetation. As for example in Figure 6 (middle row), most additional points were extracted between the top of the spruce trees and the ground. Thus, the crown base height can possibly be better estimated which could increase classification accuracy between pine and spruce trees. Also, the deciduous trees seemed not to be as dense as the spruce trees giving rise to more returns within the canopy.

5.1 Width

The width of the points ($2*\sigma_j$) was studied for area 4. In Figure 7 left, a point cloud of the area is shown where the color indicates the width of the points. For this area, the ground surface was estimated (Elmqvist, 2002) and the points were classified as ground and non-ground, i.e. vegetation (Figure 7 right).
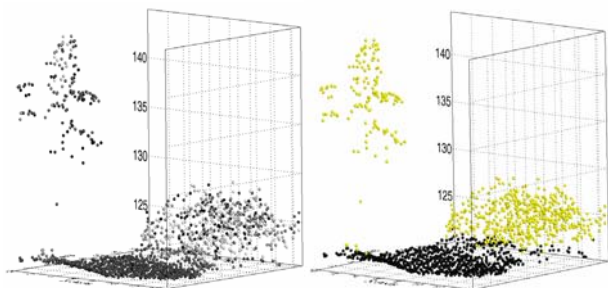

Figure 7. Area 4. Left: the color of the points indicates the width of the points. Lighter points are wider. Right: points classified as ground (black) and vegetation (gray).

The width of the ground-points was compared with the width of the vegetation-points (Figure 8). The mean width of the ground-points was 4.22 samples and mean width of the vegetation-points was 5.42 samples. On the average, the width of the vegetation-points tended to be wider.
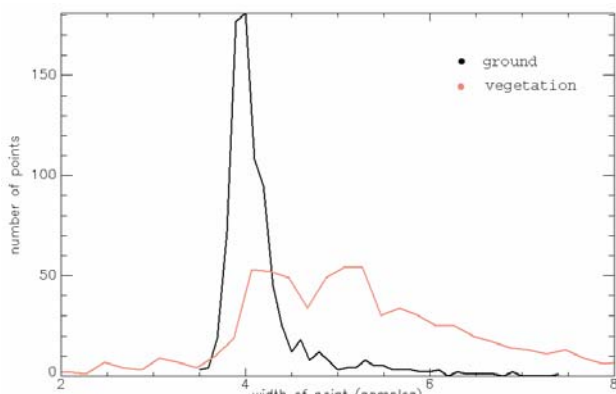

Figure 8. Histogram of width of points, ground (black), vegetation (gray).

In Figure 9, the width of the points is plotted against the intensity. The vegetation points also tended to have a lower intensity. The widening of the vegetation points and the lower

intensity may be explained by their travelling path through layers of branches compared to most ground points which directly hit a compact surface.

The received signal from ground points, which have not been affected by vegetation, should have a more similar shape to the emitted laser pulse. If instead using the full width at half maximum (FWHM) of the estimated components as the width, the mean value for the ground-points was 5.03 samples. This agrees with what could be expected since the pulse length was specified as 5 ns.
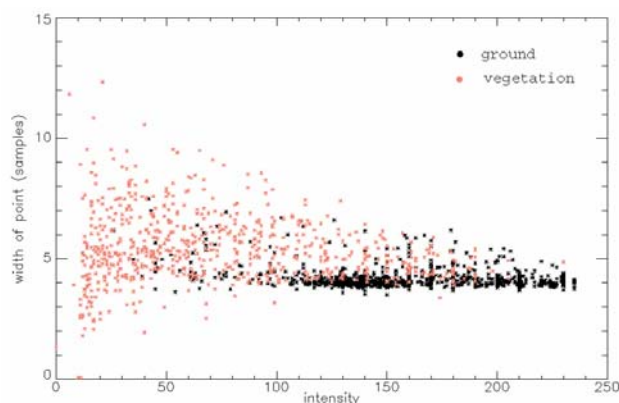

Figure 9. Width vs intensity of points, ground (black), vegetation (gray).

5.2 Range

The waveform data allows the user to study and elaborate on range estimation. The range estimated by the system occurred on the leading edge which is a few samples earlier when compared to using the mean value of the fitted Gaussian components. In (Wagner et al., 2004), different detection methods such as detection of local maxima and zero crossing of the second derivative were tested on simulated waveforms and the range errors compared. The range errors for the zero crossing of the second derivative were more accurate than the local maxima. Hence, one way to improve the accuracy of positions of the extracted points using the approach presented in this paper can be to use the zero crossing of the second derivative of the Gaussian components for defining the position of the points. This will yield more similar positions to what is used by the system.

As suggested earlier, canopy height estimations may be improved by using waveform data by detecting sub-peaks from branches on the top echo (Hug et al., 2004). In Figure 10, additional points extracted from waveform data are shown for an area with a tree. The two lines indicate the laser pulse travelling path for the two waveforms to the right. In both waveforms the last echo is the return from ground. In this example, weak echoes were detected from the top branches which were not detected by the system. The solid vertical lines illustrate the position of the points extracted by the system and the dashed vertical lines show the position of the zero crossing of the second derivative for the first component in each waveform. The highest elevation of all points extracted by the system was 131.05 m while for the points extracted from waveform data was 131.34 m (upper waveform in Figure 10). By detecting weak echoes or sub-peaks on the top echo in waveform data, the canopy height can possibly be better estimated.
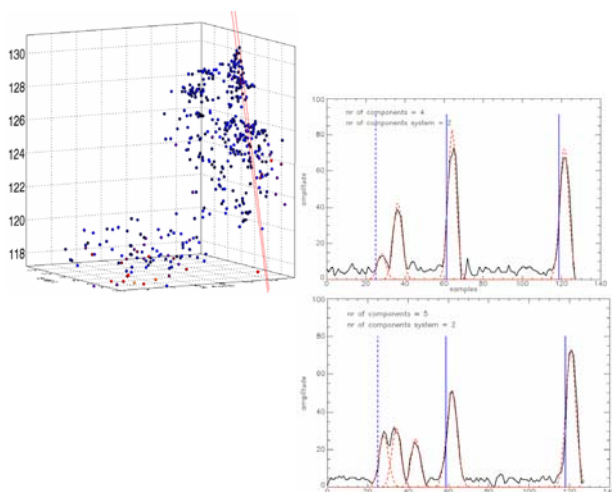
Figure 10. The additional points extracted from the waveforms (top left). The two lines indicate the travelling path for the waveforms to the right. The solid vertical lines show the position of the points extracted by the system. The dashed vertical lines show the position of the zero crossing of the second derivative for the first components. These positions correspond to a height value of 131.34 m (upper waveform) and 131.16 m (lower waveform).

6. CONCLUSIONS

Some initial processing and analysis have been performed on full-waveform airborne laser scanner data. An approach has been presented for extracting 3D point data from the waveforms. For the small forest areas presented, the number of additional points that were extracted ranged between 18-57% depending on the type of vegetation. The possibility to extract additional points can give a better description of the vertical structure of vegetation and can possibly improve tree species classification.

REFERENCES

Blair, J. B., Rabine, D. L. and Hofton, M. A., 1999. The Laser Vegetation Imaging Sensor: a medium-altitude, digitisation-only, airborne laser altimeter for mapping vegetation and topography. *ISPRS Journal of Photogrammetry & Remote Sensing*, 54, pp. 115-122.

Dempster, A. P., Laird, N. M. and Rubin, D. B., 1977. Maximum likelihood from incomplete data via the EM algorithm. *Journal of the Royal Statistical Society*, Series B, 39(1), 1-38.

Elmqvist, M., 2002. Ground surface estimation from airborne laser scanner data using active shape models, *Photogrammetric Computer Vision-ISPRS Commission III Symposium*, vol. XXXIV, part A, pp. 114-118.

Hofton, M. A., Blair, J. B. and Minster, J., 2000. Decomposition of Laser Altimeter Waveforms. *IEEE Transactions on Geoscience and Remote Sensing*, vol. 38, no 4. pp. 1989-1996.

Hug, C., Ullrich, A. and Grimm, A., 2004. LiteMapper-5600 – A Waveform-Digitizing Lidar Terrain and Vegetation Mapping System. *Proceedings of the ISPRS working group VIII/2*. Vol. XXXVI, part 8/W2. Freiburg, Germany, Oct 3-6. pp. 24-29.

Gustafsson, F., 2000. *Adaptive Filtering and Change Detection*. Wiley, pp. 125.

http://www.optech.on.ca

http://www.riegl.co.at

http://www.topeye.com

http://www.vostat.org/help/median_mad_and_quantile.html

Mitchell, T. M., 1997. *Machine Learning*. McGraw-Hill, New York, NY, pp. 191-196.

Oliver, J. J., Baxter, R. A. and Wallace, C. S., 1996. Unsupervised Learning Using MML, Machine Learning. *Proceedings of the Thirteenth International Conference (ICML'96)*, Morgan Kaufmann Publishers, San Francisco CA USA, pp. 364-372.

Steinvall, K. O., Klevebrandt, H., Lexander, J. and Widen, A., 1981. Laser depth sounding in the Baltic Sea. *Applied Optics*. 20, pp. 3284-3286.

Steinvall, K. O., Koppari, K. R. and Karlsson, U. C. M., 1994. Airborne laser depth sounding. System aspects and performance. *In Ocean Optics XII*, J. S. Jaffe, ed., Proc. SPIE 2258, pp. 392-412.

Tulldahl, H. M., Andersson, M. and Steinvall, K. O., 2000. Experimental results of small target detection in airborne laser depth sounding, presented at the Ocean Optics XV Conference, Monaco, France, 16-20 Oct. 2000.

Wagner, W., Ullrich A., Melzer T, Briese C. and Kraus K., 2004. From single–pulse to full-waveform airborne laser scanners: Potential and practical challenges. *ISPRS XXth Congress*, Istanbul, Vol XXXV, Part B/3, pp. 201-206.

Wehr, A. and Lohr, U. 1999. Airborne laser scanning – an introduction and overview, *ISPRS Journal of Photogrammetry & Remote Sensing*, 54, pp. 68-82.